THE *HERSCHEL*-ATLAS DATA RELEASE 2 – PAPER 2: CATALOGUES OF FAR-INFRARED AND SUBMILLIMETRE SOURCES IN THE FIELDS AT THE SOUTH AND NORTH GALACTIC POLES

S.J. Maddox,[1, 2] E. Valiante,[1] P. Cigan,[1] L. Dunne,[1, 2] M. W. L. Smith,[1] S. Eales,[1] S. Dye,[3] C. Furlanetto,[3, 4] E. Ibar,[5] G. de Zotti,[6] J. S. Millard,[1] N. Bourne,[2] H. L. Gomez,[3] R. J. Ivison,[7] and I. Valtchanov[8]

[1] *School of Physics and Astronomy, Cardiff University, The Parade, Cardiff CF24 3AA, UK.*

[2] *Institute for Astronomy, The University of Edinburgh, Royal Observatory, Blackford Hill, Edinburgh, EH9 3HJ, UK.*

[3] *School of Physics and Astronomy, University of Nottingham, University Park, Nottingham, NG7 2RD, UK.*

[4] *Departamento de Fisica, Universidade Federale do Rio Grande do Sul., Av. Bento Goncalves, 9500, 91501-970, Porto Algres, RS Brazil*

[5] *Instituto de Física y Astronomía, Universidad de Valparaíso, Avda. Gran Bretaña 1111, Valparaíso, Chile.*

[6] *INAF-Osservatorio Astronomico di Padova, Vicolo dellâĂŹOsservatorio 5, I-35122 Padova, Italy*

[7] *European Southern Observatory, Karl-Schwarzschild-Strasse 2, 85748, Garching, Germany*

[8] *European Space Agency*

ABSTRACT

The *Herschel* Astrophysical Terahertz Large Area Survey (H-ATLAS) is a survey of 660 deg^2 with the PACS and SPIRE cameras in five photometric bands: 100, 160, 250, 350 and 500 μm. This is the second of three papers describing the data release for the large fields at the south and north Galactic poles (NGP and SGP). In this paper we describe the catalogues of far-infrared and submillimetre sources for the NGP and SGP, which cover 170 deg^2 and 285 deg^2, respectively. The catalogues contain 112,074 sources for the NGP field and 193,536 sources for the SGP field detected at more than 4σ significance in any of the 250, 350 or 500 μm bands. The source detection is based on the 250 μm map, and we present photometry in all five bands for each source, including aperture photometry for sources known to be extended. The rms positional accuracy for the faintest sources is about 2.4 arc seconds in both right ascension and declination. We describe a statistical analysis of the catalogues and discuss the practical issues – completeness, reliability, flux boosting, accuracy of positions, accuracy of flux measurements – necessary to use the catalogues for astronomical projects.

Keywords: methods: data analysis - catalogues - surveys - galaxies: statistics - cosmology: observations - submillimetre: galaxies

1. INTRODUCTION

This is the second of three papers describing the second major data release of the *Herschel* Astrophysical Terahertz Large Area Survey (the *Herschel* ATLAS or H-ATLAS), the largest single key project carried out in open time with the *Herschel Space Observatory*[1] (Pil-

Corresponding author: S. J. Maddox
maddoxs@cardiff.ac.uk

[1] *Herschel* is an ESA space observatory with science instruments provided by European-led Principal Investigator consortia and with important participation from NASA

bratt et al. 2010). The H-ATLAS is a survey of approximately 660 deg^2 of sky in five photometric bands: 100, 160, 250, 350 and 500 μm (Eales et al. 2010). Although the original goal of the survey was to study dust, and the newly formed stars hidden by dust, in galaxies in the nearby ($z < 0.4$) universe (Dunne et al. 2011, Eales et al. 2018), in practice the exceptional sensitivity of *Herschel*, aided by the large negative k-correction at submillimetre wavelengths (Franceschini et al. 1991), has meant that the median redshift of the sources detected in the survey is approximately 1 (Pearson et al. 2013), and our source

catalogues include sources up to a redshift of at least 6 (Fudamoto et al. 2017; Zavala et al. 2017).

The five H-ATLAS fields were selected to be areas with relatively little emission from dust in the Milky Way, as judged from the IRAS 100 μm images (Neugebauer 1984), and with a large amount of data in other wavebands. In 2010 for the Science Demonstration Phase (SDP) of *Herschel*, we provided the data products for one 16 deg^2 field in the GAMA 9-hour field (Ibar et al. 2010; Pascale et al. 2011; Rigby et al. 2011; Smith et al. 2011). In our first large data release (DR1), we released the data products for three fields on the celestial equator centred at R.A. approximately 9, 12 and 15 hours (Valiante et al. 2016, hereafter V16; Bourne et al. 2016), covering a total area of 161 deg^2. These data products included the *Herschel* images in all five bands, a catalogue of the 120,230 sources detected in these images and of the 44,835 optical counterparts to these sources.

Our second data release is for the two larger fields at the north and south Galactic poles (NGP and SGP). The NGP field is centred approximately at a right ascension of 13^h 18^m and a declination of +29° 13′ (J2000) and has an area of 180.1 deg^2. The NGP field is a roughly square region (Fig. 1) and, among many other interesting known extragalactic objects, includes the Coma Cluster. The SGP field is centred approximately at a right ascension of 0^h 6^m and a declination of −32° 44′ (J2000) and has an area of 317.6 deg^2. The SGP field is elongated in right ascension (Fig. 2). Smith et al. (2017, hereafter S17) provide a comprehensive list of the multi-wavelength data that exist for these fields.

Our data release for these fields is described in three papers. In the first paper (S17), we present the images of these fields, including a description of how these images can be used by the astronomical community for a variety of scientific projects. In this paper, we describe the production and properties of the catalogues of far-infared and submillimetre sources detected in these images. A third paper (Furlanetto et al. 2017, hereafter F17) describes a search for the optical/near-infrared counterparts to the *Herschel* sources in the NGP field and the resulting multi-wavelength catalogue.

The arrangement of this paper is as follows. Section 2 describes the detection of the sources. Section 3 describes the photometry of the sources. Section 4 describes the catalogues and their properties. Finally Section 5 gives a summary of the paper.

The catalogues described in this paper can be obtained from the H-ATLAS website (http://www.h-atlas.org). Note that since we only search for sources where the images are made out of more than one individual

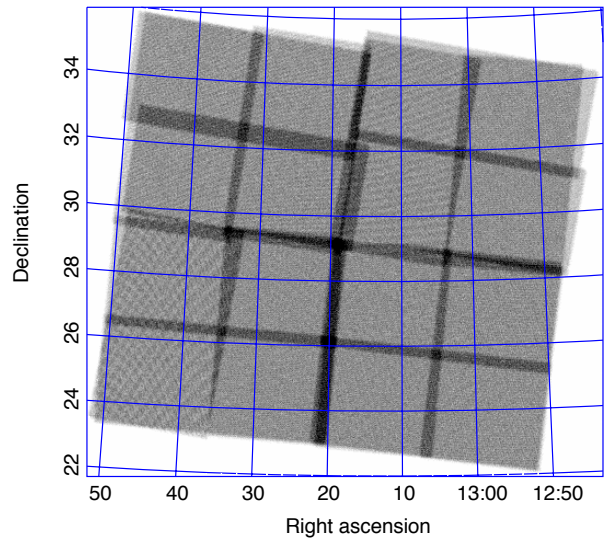**Figure 1.** The coverage map for 250 μm observations of the NGP field. The map shows the number of samples from the bolometer timelines contributing to each map pixel, which ranges from 1 to 43, with the median value being 10. The range of the grayscale is from 0 samples (white) to 27 samples (black).

Herschel observation, the area covered by the catalogues (170 deg^2 and 285 deg^2 for the NGP and SGP, respectively) is slightly smaller than the sizes of the maps (180.1 deg^2 and 317.6 deg^2, respectively - S17). Also, the SPIRE and PACS photometers are offset by 21 arcmin, which creates regions around the borders that are covered by only one of the two photometers. As in previous data releases we restrict our catalogues to the area covered by the 250 μm maps.

2. SOURCE DETECTION

2.1. *The maps and background subtraction*

A detailed description of the processing necessary to produce maps from the *Herschel* raw data is presented in S17. The resulting maps have pixel sizes 3, 4, 6, 8 and 12 arc seconds for 100, 160, 250, 350 and 500 μm respectively. Note that these are different to the canonical pixel sizes used for maps in the *Herschel* Science Archive, which use 3.2, 3.2 6, 10 and 14 arc seconds respectively. The maps made with the PACS camera (100 and 160 μm, Poglitsch et al. 2010) have units of Jy per pixel. The maps made with the SPIRE camera (250, 350 and 500 μm, Griffin et al. 2010) have units of Jy per beam. The beam areas at 250, 350 and 500 μm are 469, 831 and 1804 square arc seconds, respectively (Valtchanov 2017). The noise on the images is a combination of instrumental noise and the confusion noise from sources that are too faint to be detected individu-
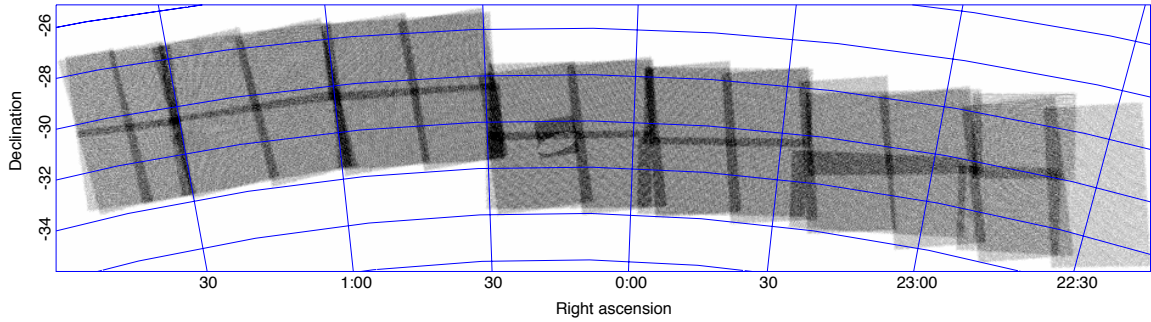
Figure 2.   The coverage map for $250\,\mu$m observations of the SGP field. The map shows the number of samples from the bolometer timelines contributing to each map pixel, which ranges from 1 to 36, with the median value being 9. The range of the grayscale is from 0 samples (white) to 21 samples (black).

ally. S17 describes a detailed analysis of the noise properties of the images.

Before attempting to detect sources in the maps, we first subtracted a smoothly varying "sky" level to remove the foreground emission from dust in our galaxy, so-called "cirrus emission", and also the emission from clustered extragalactic sources fainter than our detection limit. We used the `nebuliser` function, a programme produced by the Cambridge Astronomy Survey Unit to estimate and subtract the sky level on astronomical images[2].

The choice of the filter scale used in `nebuliser` is quite critical, since it must be small enough for `nebuliser` to remove small-scale patches of cirrus emission but not so small that the flux from large galaxies is reduced. In practice, for the SPIRE maps we found that a median filter scale of 30 pixels (3 arc minutes in the $250\,\mu$m band) followed by a linear filter scale of 15 pixels was an acceptable combination.

We tested whether this filtering scale reduced the flux density of extended extragalactic sources by creating simulated maps, placing artificial extended sources on these maps, and then measuring the flux densities of these sources after the application of `nebuliser`. Since the nearby galaxies detected by *Herschel* are mostly spiral galaxies, we used exponential profiles for the artificial sources, convolving these with the SPIRE point-spread function. The surface-brightness limit on photographic plates is typically $\mu_{\rm B} \simeq 25$ mag arcsec^{-2}, giving rise to the widely used D25 optical diameters for galaxies. Since these diameters are roughly equivalent to a distance of five scale lengths from the centre of a galaxy, we truncated the profiles of our artificial submillimetre sources at five scale lengths, which gave us diameters, roughly

equivalent to D25 diameters in the optical waveband, which ranged from 24 to 192 arcsec. The simulations showed that significant flux is lost only for sources that have diameters larger than 3 arc minutes, and even for sources above this size, the flux loss is $\lesssim 10\%$. Note there are only 12 galaxies with diameter larger than 3 arc minutes in the survey: 3 in the NGP and 9 in the SGP.

We note that the application of `nebuliser` will change the clustering statistics of extragalactic sources. Apart from the foreground cirrus emission, `nebuliser` removes the background produced by the sources that are too faint to be detected individually. This background varies because of the clustering of these faint sources.   A source catalogue made without any background subtraction will include more sources where this background is high as a result of clusters of these faint sources, and so the clustering of the sources in such a catalogue will be stronger than in a catalogue produced from an image in which this background emission has been removed. An investigation of the clustering in the H-ATLAS catalogues, which includes an analysis of the effect of the subtraction of this background, will be presented by Amvrosiadis et al. (in preparation).

For the PACS maps, the $1/f$-noise from the instrument is much larger than for SPIRE, making the foreground cirrus emission and the background emission from faint galaxies difficult to detect. Since we could not clearly detect the foreground/background emission on smaller scales, we used a `nebuliser` scale of 5 arcminutes.

The raw maps from the SPIRE pipeline have a mean of zero, but the output maps from `nebuliser` have a modal pixel value that is zero. For the SPIRE bands, the instrumental noise is low enough that the flux distribution of detected sources skews the pixel distribution to positive values so the mean is slightly positive

(1.0, 1.0 and 0.6 mJy/beam at 250, 350 and 500 μm). The PACS detector is less sensitive and less stable than SPIRE, and so the instrumental noise dominates over the confusion noise and the pixel distribution is close to Gaussian; the mean of the `nebulised` PACS maps are very close to zero (0.016 MJy sr^{-1}, for both the 100 and 160 μm maps).

2.2. *Source Detection*

In this section we describe the method used to find the sources on the images. Additional details are given in V16. Sources were detected using the `MADX` algorithm (Maddox et al in prep) applied to the SPIRE maps. `MADX` creates maps of the signal-to-noise ratio and identifies sources by finding peaks in the signal to noise. The detection and measurement of fluxes is optimised by using a matched filter that is applied to both the signal map and the noise map.

The SPIRE instrumental noise maps are created from the number of detector passes and the estimated instrumental noise per pass, $\sigma_{\text{inst}}/\sqrt{N_{\text{sample}}}$, as described in S17 and V16.

Since the noise consists of both instumental noise and confusion noise from the background of undetected sources, we follow the approach of Chapin et al (2011) to calculate the optimal matched filter in each of the three SPIRE bands. Details of the estimation and form of the matched filter are discussed in V16. The resulting matched filters are slightly more compact than the corresponding PSFs, and have slightly negative regions outside the FWHM.

In the first step of the source detection, peak pixels which have values $> 2.5\sigma$ in the filtered 250-μm map are considered as potential sources. We use the 250-μm map since most sources have the highest signal-to-noise in this map. The source position is determined by fitting a Gaussian to the flux densities in the pixels surrouding the pixel containing the peak emission. As an initial estimate of the flux density of the source in each SPIRE band, `MADX` takes the flux density in the pixel closest to the 250-μm position.

The high source density on the SPIRE maps means that these flux estimates often contain contributions from neighbouring sources. To mitigate this effect, `MADX` uses the following procedure. In each band, `MADX` sorts the sources in order of decreasing flux density. The flux density of the brightest source is then more precisely estimated using the value of the filtered map interpolated to the exact (sub-pixel) position from the 250-μm map. Using this flux estimate, a point source profile is then subtracted from the map at this position. Since the bright source is now removed from the map, any fainter

sources nearby should have fluxes that are not contaminated by the brighter source. The program then moves to the next brightest source and follows the same set of steps. One consequence of these steps is that some sources will now have 250-μm flux densities less than the original 2.5σ cut. Since most sources are brighter at 250μm than at the two longer wavelengths, the estimates of the flux densities in the 350-μm and 500-μm bands are on average significantly lower in signal to noise, and can even sometimes be negative. We retain these negative measurements so that the distribution of fluxes in the catalogues is consistent with the errors, and not truncated at an arbitrary limit.

3. PHOTOMETRY

3.1. *Point sources*

3.1.1. *SPIRE*

V16 carried out extensive simulations to determine the errors on the flux density estimates for point sources. They followed the simple procedure of injecting artificial sources of known flux density into the real maps and then using `MADX` to estimate their flux densities (Section 2.2). They found that at 250 μm, the detection wavelength, the confusion noise varies as a function of source flux density and gave a simple formula to approximate this:

$$\sigma_{\text{con250}} = \sqrt{\min(0.0049, f_{250}/5.6)^2 + 0.00253^2} \;\; \text{Jy}. \;\; (1)$$

They found that at 350 μm and 500 μm the confusion noise is roughly constant, with $\sigma_{\text{con350}} = 0.00659$ Jy and $\sigma_{\text{con500}} = 0.00662$ Jy.

We calculated the errors in the flux density estimates for each individual source, using these formulae to estimate the confusion noise and the maps of the instrumental noise (Section 2.2) to estimate the instrumental noise, then adding the confusion and instrumental noise in quadrature.

Our strategy of creating the H-ATLAS survey from overlapping tiles (S17) means that the instrumental noise varies systematically between different areas of the maps. Figure 3 shows histograms of instrumental noise and total noise (instrumental noise plus confusion noise) for all pixels and at the positions of all sources. The multiple peaks are the results of our tiling strategy. The main peak corresponds to the large fraction of the survey area that was covered by two individual *Herschel* observations (S17). The smaller peaks at lower noise correspond to the smaller fraction of the survey area that was covered by more than two observations. The small peak at higher noise in the SGP field corresponds
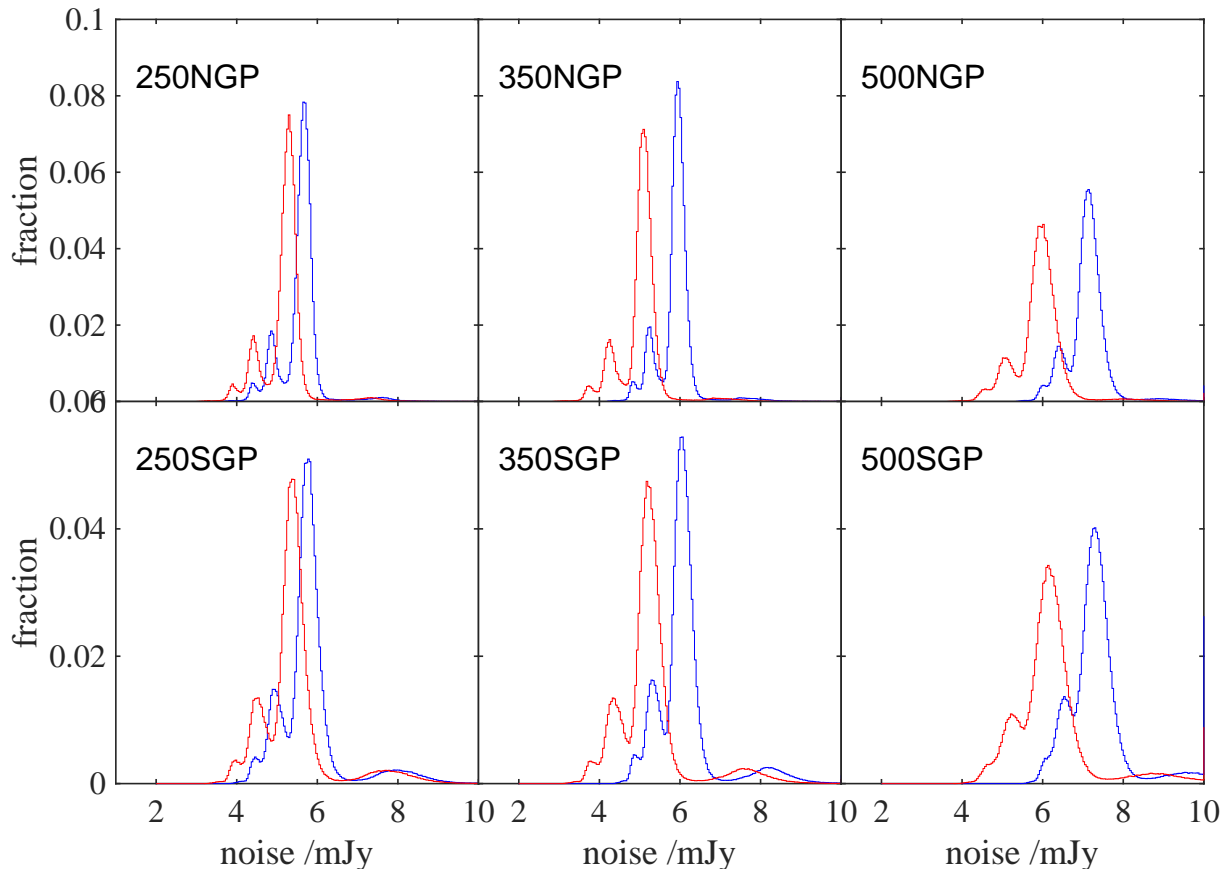
Figure 3. The distribution of instrumental and total noise for the 250-μm, 350-μm and 500-μm bands for the NGP and SGP fields. Green shows the instrumental noise and black the total noise for all pixels; red shows the instrumental noise and blue the total noise at the positions of all sources. The multiple peaks are the results of our tiling strategy. The main peak corresponds to the large fraction of the survey area that was covered by two individual *Herschel* observations (S17). The smaller peaks correspond to the small fraction of the survey area that was either covered by more than two observations or, in the case of one end of the SGP (S17), a single observation (the small peak at the right in the bottom panels.

to the area at the western end that was covered by a single observation (S17).

The variation of noise across the maps means that the 4σ flux-density limit varies over the fields, and hence the available area depends on the chosen flux density limit. Figure 4 shows the relationship between area and flux-density limit for each of the H-ATLAS fields, including the GAMA fields.

3.1.2. *PACS*

As in V16, we used aperture photometry to estimate the flux densities in the two PACS bands. We did this for two reasons. First, the PACS PSF for our observing mode (fast-parallel scan mode) is not well determined near its peak (see V16 for an extensive discussion). Second, if we estimated the 100- and 160-μm flux densities at the 250-μm position, as we did for the 350- and 500-

μm bands, we would be likely to significantly underestimate the flux density because of the higher resolution of the PACS maps.

V16 describes an extensive investigation of the optimum aperture size, and we follow that paper in using an aperture with a radius equal to the FWHM, which is 11.4 arc seconds for 100 μm and 13.7 arc seconds for 160 μm. Although the "sky" level has already been subtracted with `nebuliser`, we subtracted the mean value from each image before carrying out the photometry, to ensure that the statistical properties of the sources in the catalogues are not affected by any residual errors in the sky subtraction. To provide an accurate treatment of the contribution from fractional pixels near aperture boundaries, we divided each pixel into 16, and assigned one sixteenth of the flux density in each sub-pixel, corresponding to a nearest-pixel interpolation. Then the flux
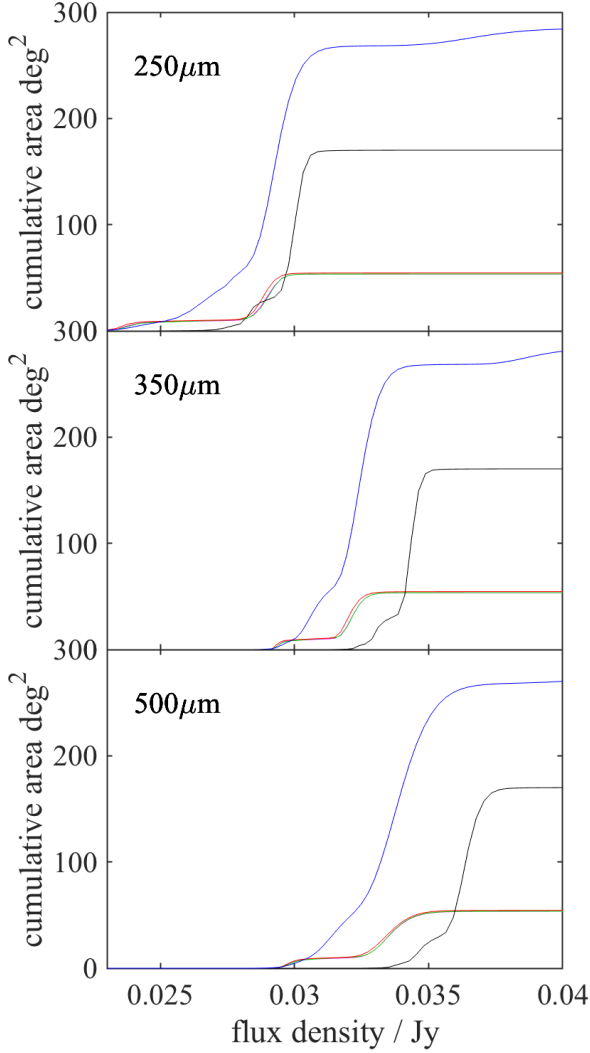
Figure 4. The relationship between area and 4σ flux-density limit for the H-ATLAS fields: NGP - black; SGP - blue; GAMA9 - magenta; GAMA12 - green and GAMA15 - cyan. The more sensitive areas correspond to the tile overlaps in each field. The westerly end of SGP has only a single SPIRE observation, which explains the kink at high flux densities in the blue line in these panels.

density from each sub-pixel that lies within the aperture is added together to produce the total aperture flux. We also tried bilinear, and bicubic interpolation methods and found negligible differences in the resulting aperture fluxes. Since only $\simeq 10\%$ of the SPIRE sources were clearly detected on the PACS images, we centred the aperture on the 250-μm position.

We corrected the aperture flux densities to total flux densities using the table of the encircled energy fraction (EEF) described in V16 and available at http://www.h-atlas.org/. We made a further correction to allow for the effect of the errors on the 250-μm positions, since any error in the position will lead to the small PACS apertures missing flux. V16 describes simulations of this effect, and we follow that paper in compensating for this effect by multiplying the flux densities by 1.1 and 1.05 at 100 and 160 μm, respectively.

We describe how we estimated the errors on these flux estimates in the following subsection.

3.2. *Extended sources*

The approach in Section 3.1 gives optimal flux density estimates for point sources, but will substantially underestimate the flux density of extended sources. As in V16, we used the r−band sizes of optical counterparts to the *Herschel* sources to indicate which sources are likely to require aperture photometry rather than the methods described in the last section. We followed different methods for the NGP and the SGP because of the lack of a comprehensive identification analysis for the SGP. We estimate aperture photometry for extended sources in both PACS and SPIRE bands.

3.2.1. *The NGP*

In the NGP, F17 carried out a search for optical counterparts to the *Herschel* sources on the r-band images of the Sloan Digital Sky Survey (SDSS) which was almost exactly the same as that carried out by Bourne et al. (2016) for the H-ATLAS GAMA fields. Our initial list of NGP sources that might require aperture photometry were the sources with optical identifications with reliability $R > 0.8$ from F17.

In our previous data release (V16) we calculated the sizes of our apertures from the SDSS parameter `isoA_r`, which was available in SDSS DR7. However, this parameter was not available in SDSS DR10, on which F17 based their analysis. After an investigation of the various size measurements available in DR10, we found that the parameter `petroR90_r`, the 90% Petrosian radius, met our needs since there is a simple scaling between it and `isoA_r`, with `isoA_r` $\simeq 1.156$ `petroR90_r`. The scale-factor 1.156 is derived from a simple fit to `isoA_r` as a function of `petroR90_r`.

We considered that for H-ATLAS sources with optical counterparts with `petroR90_r` less than 8.6 arcsec (equivalent to the value of `isoA_r` of 10 arcsec used in V16), the source is still unlikely to be extended in the SPIRE bands, and for these H-ATLAS sources we preferred to adopt the flux densities in the SPIRE bands produced by `MADX` (Section 3.1.1). However, if the H-ATLAS source had an optical counterpart with

`petroR90_r` greater than 8.6 arcsec, we measured aperture photometry for the SPIRE bands. We calculated the radius of the aperture using the same formula as V16 (with `isoA_r` replaced by `petroR90_r`):

$$r_{ap} = \sqrt{FWHM^2 + (1.156 \, \texttt{petroR90\_r})^2} \,, \qquad (2)$$

where `FWHM` is the full-width at half-maximum of the point-spread function for the passband being measured, and all radii are measured in arc seconds. As discussed above (Section 3.1.2), we also use aperture photometry in the PACS bands for sources without reliable optical counterparts, using an aperture with a radius equal to the FWHM.

After calculating the aperture using equation 2, we visually compared it with the 250-μm emission from the source, since in some case the aperture is not well-matched to the 250-μm emission, either being too small, too large, with the wrong shape or including the flux from a neighbouring galaxy (see V16 for examples). In these cases, we chose a more appropriate aperture for the galaxy, which may involve changing the radius or changing to an elliptical aperture. We also visually inspected the 3000 sources with the brightest 250-μm flux densities from `MADX` in order to check whether there were any obvious additional extended sources. For these sources too, we chose appropriate apertures to include all of the emission. In total, for the NGP there are 77 of these "customised apertures". The semi-major, semi-minor axes and position angles of these customised apertures are given as part of the data release.

We centered the apertures on the optical positions, since these are more accurately determined than the *Herschel* positions. Although the "sky" level on both the PACS and SPIRE images has already been subtracted with `nebuliser`, we subtracted the mean value from each image before carrying out the photometry, in order to avoid residual errors in the sky subtraction affecting the statistical properties of the catalogues. As describe in Section 3.1.2, we divided each pixel into 16, assigning one sixteenth of the flux density in each sub-pixel, and added up the flux density in each sub-pixel within the aperture. We corrected the PACS flux densities to total flux densities using the table EEF described in V16 and available at http://www.h-atlas.org/. We corrected all the SPIRE aperture flux densities for the fraction of the PSF outside the aperture using a table of corrections determined from the best estimate of the SPIRE PSF (Griffin et al. 2013, Valtchanov 2017), which is provided as part of the data release (see V16 for more details).

We calculated errors in the aperture flux densities from the results of the Monte Carlo simulation of S17.

S17 placed apertures randomly on the SGP and NGP maps in areas that are made from two individual observations ($N_{scan} = 2$), varying the aperture radii from approximately the beam size up to 100 arc seconds in 2 arc second intervals and using 3000 random positions for each aperture radius. They found that the error, σ_{ap} in mJy, depends on the radius the aperture as a double power-law:

$$\sigma_{ap}(mJy) = \begin{cases} Ar^\alpha, & \text{if } r \le 50'', \\ B(r-50)^\beta + A50^\alpha, & \text{for } r > 50''. \end{cases} \qquad (3)$$

The constants A, B, α, and β are given in Table 3 of S17. We used this equation for the sources on parts of the images made from two observations. In parts of the images made from more than two observations the instrumental noise is less; for sources in these more sensitive parts of the images we used the extensions of equation 3 derived by S17; i.e. equation 4 in S17 for SPIRE and equation 6 in S17 for PACS.

Finally, we only used the aperture flux density if it is significantly larger than the point-source estimate, i.e.

$$F_{ap} - F_{ps} > \sqrt{\sigma_{ap}^2 - \sigma_{ps}^2} \,. \qquad (4)$$

In summary, of the 118,986 sources in the NGP, we measured aperture flux densities at 250 μm for 889 sources.

3.2.2. *The SGP*

For the SGP area no SDSS data exist and we have not carried out the comprehensive identification analysis that we performed for the other four fields. Instead, we have carried out a rudimentary identification analysis using the 2MASS survey (Skrutskie et al. 2006). We first found a 2MASS galaxy parameter that provides a useful estimate of the size of the galaxy. We found that the 2MASS parameter "super-coadd 3-sigma isophotal semi-major axis", `sup_r_3sig`, has a simple scaling with the `isoA_r`: `isoA_r` $\simeq 1.96$ `sup_r_3sig`. The scale-factor 1.96 is derived from a simple fit to `isoA_r` as a function of `sup_r_3sig`.

We found all 2MASS galaxies in the SGP region with `sup_r_3sig` > 5.1 arcsec, equivalent to `isoA_r` = 10 arcsec. There are 6249 of these galaxies. We then found all H-ATLAS sources in the SGP within 5 arcsec of a 2MASS galaxy. There are 3444 of these sources. We used the surface-density of Herschel sources to estimate the probability of a Herschel source falling within 5 arcsec of a 2MASS galaxy by chance; we estimate that only 23 (0.7%) of these matches should not be physical associations of the H-ATLAS source and the 2MASS galaxy.

For these sources, we calculated the radius of the aperture to use for photometry using the relationship:

$$r_{\mathrm{ap}} = \sqrt{\mathtt{FWHM}^2 + (1.96\ \mathtt{sup\_r\_3sig})^2}\ . \qquad (5)$$

This is the same as equation 2, except for the change in the parameter used to estimate the size of the galaxy. In principle we could use `sup_r_3sig` as our radius measure for the sources in the NGP, but SDSS is significantly deeper than 2MASS and so the measurements are likely to have smaller uncertainties.

As for the NGP, we then visually compared the apertures with the 250-μm emission from the source, modifying the aperture when necessary (see above). We also visually inspected the 5000 sources with the brightest 250-μm flux densities from `MADX` in order to check whether there were any obvious additional extended sources. For these sources, we also chose appropriate apertures to include all of the emission. In total, for the SGP there are 142 customised apertures, for which the details are given as part of the data release.

In the case of the SGP, we centered the apertures on the 250-μm positions rather than on the optical positions. Otherwise we followed exactly the same procedures to estimate the fluxes and errors as for the NGP, described in Section 3.2.1. In summary, of the 118,986 sources in the SGP, we measured aperture flux densities at 250 μm for 1452 sources.

3.3. *Comparison to Planck photometry*

Estimating the flux density of extended sources is sensitive to the background subraction and choice of aperture size, so it is useful to compare our extended source fluxes to other measurements available. In particular for the 350 μm and 500 μm bands, we have compared to the compact source catalogue from the Planck survey (Planck Collaboration XXVI, 2016). Given the low-surface density of sources, a simple positional match is sufficient to cross-identify sources in common. We find 44 matches in the NGP, as plotted in Figure 5. We have adopted the *Planck* APERFLUX photometry as recommended by Planck Collaboration XXVI (2016) for these wavelenghts. The *Planck* 545 GHz (550 μm) flux densities, and their errors, have been scaled up by a factor of 1.35 to convert them to 500 μm.

As seen in Figure 5, there is a very good corespondence between the measurements wih no significant systematic offsets of non-linearities. Also, the scatter between the measurements is consistent with the quoted uncertainties.

The estimated 90% completeness limit of the Planck 350micron catalogue in the 'extragalactic zone' (|b|>

30deg) given by Planck Collaboration XXVI (2016) is 791 mJy; the comparison with the HATLAS NGP catalogue suggests 90% completeness down to F350BEST=650 mJy. So the quoted Planck limit seems quite conservative. The number of Planck detections at 550micron is too small to derive solid conclusions. However, again the estimated completeness limit (555 mJy, corresponding to 749 mJy at 500 μm) looks conservative: Planck has detected all HATLAS NGP sources with F500BEST > 400 mJy, but there are only 9 sources above this limit.

3.4. *Colour corrections and flux calibration*

The large wavelength range within each of the SPIRE pass bands means that both the size of the PSF and the power detected by SPIRE depend on the spectral energy distribution of the source. The SPIRE data-reduction pipeline and ultimately our flux densities are based on the assumption that the flux density of a source varies with frequency as ν^{-1}. If the user knows the SED of a source, the flux densities should be corrected using corrections from either table 5.7 or 5.8 from the SPIRE handbook[3] (Valtchanov 2017). It is important to apply these corrections, since they can be quite large: for a point source with a typical dust spectrum ($T = 20$K, $\beta = 2$) the multiplicative correction is 0.96, 0.94 and 0.90 at 250, 350 and 500 μm, respectively. The catalogue fluxes have had no colour correction applied.

As with SPIRE, the PACS flux densities are also based on the assumption that flux density of the source is proportional to ν^{-1}, and a correction is required for sources which follow a different SED. The required corrections are described in the PACS Colour-Correction document[4].

On top of all other errors, there is an additional error due to the uncertain photometric calibration of *Herschel*. As in V16, we assume conservative calibration errors of 5.5% for the three SPIRE wavebands and 7% for PACS (see V16 for more details).

4. THE CATALOGUES

We included all sources in the catalogues if they were detected above 4σ in one or more of the three SPIRE bands: 250, 350 and 500 μm. We eliminated all sources from the original list of point sources produced by `MADX` if they fell within the aperture of an extended source. All of the H-ATLAS fields were observed at least twice, making it possible to search for moving sources such as

---

[3]   http://herschel.esac.esa.int/Docs/SPIRE/spire_handbook.pdf

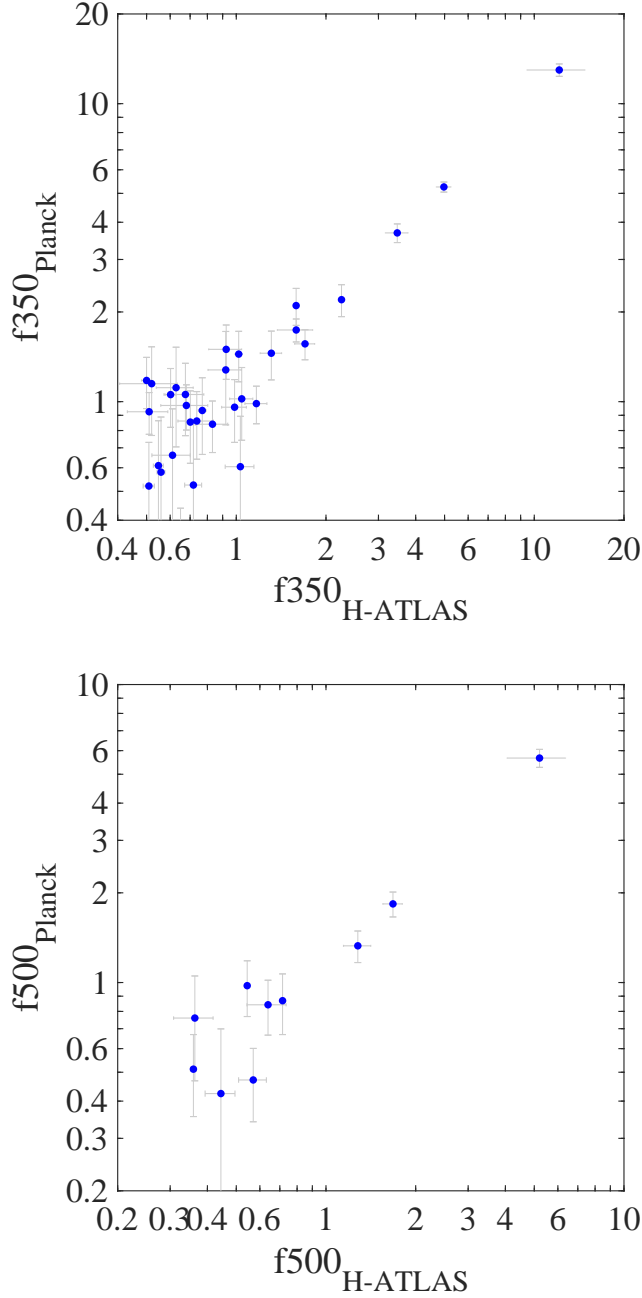[4]   http://herschel.esac.esa.int/twiki/pub/Public/PacsCalibrationWeb/cc_report_v1.pdf

Table 1. Stars in H-ATLAS

Name	Position
EY Hya	08:46:21.4 +01:37:53
IN Hya	09:20:36.7 +00:10:53
NU Com	13:10:08.5 +24:36:02
19 PsA	22:42:22.3 −29:21:43
V PsA	22:55:19.9 −29:36:48
S Sci	00:15:22.4 −32:02:44
XY Sci	00:06:35.9 −32:35:38
eta Sci	00:27:55.9 −33:00:27
Y Sci	23:09:05.7 −30:08:04
HD 119617	13:43:35.2 +35:20:45
R Sci	01:26:58.2 −32:32:37
Fomalhaut	22:57:39.2 −29:37:22

Figure 5. Comparison between H-ATLAS and Planck flux density measurements for $350\,\mu m$ and $500\,\mu m$ bands.

asteroids. We found nine asteroids in the GAMA fields (V16), eliminating these from the final catalogue. We carried out the same search for the NGP and SGP but found no moving objects.

The sources in the final catalogues are almost all extragalactic sources. We carried out a search for clusters of sources in all the H-ATLAS fields (Eales et al. in preparation). In the GAMA9 field, we found several groups of sources that are likely to be clusters of prestellar cores, implying that the catalogue for this field is likely to contain a few tens of Galactic sources. However, we found no similar clusters in the other fields, which makes sense, since the GAMA9 field is at a much lower Galactic latitude than the other fields. Prestellar cores are therefore likely to be a very minor contaminant to the catalogues for these fields. There are a few debris disks and AGB stars in the catalogues, and an incomplete list is given in Table 1. However, well over 99% of the sources are extragalactic. The extragalactic sources range from galaxies at redshift 6 (Fudamoto et al. 2017) to nearby galaxies, such as the spectacular spiral galaxy, NGC 7793, which is in the centre of the SGP, and one of the brightest galaxies in the nearby Sculptor group.

4.1. *Statistics of the catalogues*

The catalogue for the NGP contains 118,986 sources, of which 112,074 were detected at $> 4\sigma$ at 250 μm, 46,872 at $> 4\sigma$ at 350 μm and 10,369 at $> 4\sigma$ at 500 μm. The effective sensitivity of the PACS images was much less, but the catalogues contain flux-density measurements at 100 μm and 160 μm for all the sources in the catalogue. 4,207 sources were detected at $> 3\sigma$ at 100 μm and 6,342 sources were detected at $> 3\sigma$ at 160 μm.

The catalogue for the SGP contains 193,536 sources, of which 182,210 were detected at $> 4\sigma$ at 250 μm, 74,061 at $> 4\sigma$ at 350 μm and 16,076 at $> 4\sigma$ at 500 μm. 5500 sources were detected at $> 3\sigma$ at 100 μm and 10,86 sources were detected at $> 3\sigma$ at 160 μm.
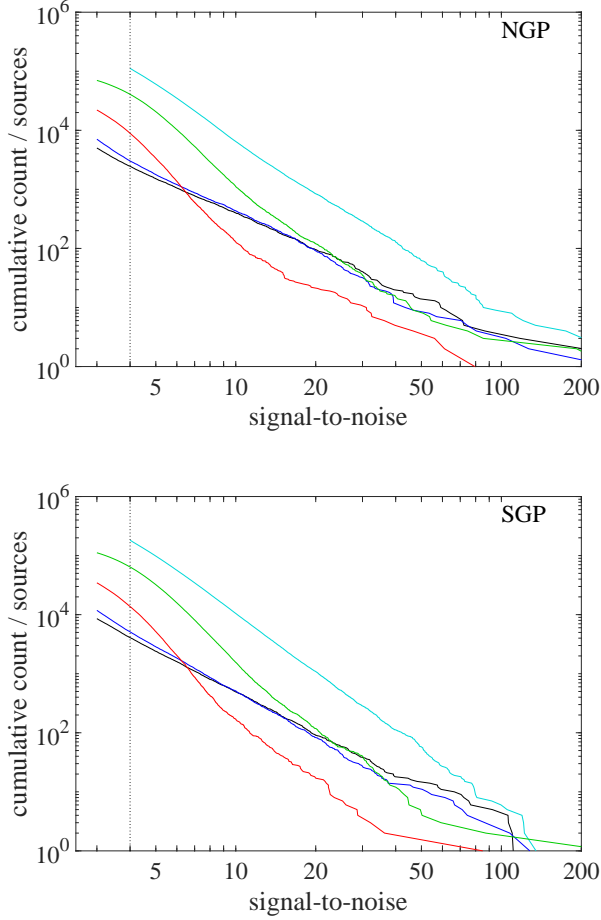
Figure 6. The cumulative number of sources as a function of signal-to-noise at $100\,\mu$m (black), $160\,\mu$m (blue), $250\,\mu$m (cyan), $350\,\mu$m (green) and $500\,\mu$m (red). The NGP area is shown in the top panel, and the SGP in bottom panel. The vertical dotted line shows the 4-σ limit for the $250\,\mu$m selection. The other bands are truncated at 3-σ.

The cumulative number of sources as a function of signal-to-noise in the five bands is shown in Figure 6. The 250-μm band is the most sensitive, and so has the largest number of detected sources. Of the PACS bands, the 160-μm band detects most sources above 3-σ.

The observed number of sources as function of flux density in the PACS and SPIRE bands is shown in Figure 7. Note that this is the observed flux in the catalogue, before any corrections are made for source SED (Section 3.3) or "flux boosting" (Section 4.3), which are necessary before the flux densities are compared with model predictions.

4.2. Positional Accuracy

V16 carried out extensive simulations to investigate the accuracy of the H-ATLAS catalogues by injecting artificial sources on to the GAMA images, and then using
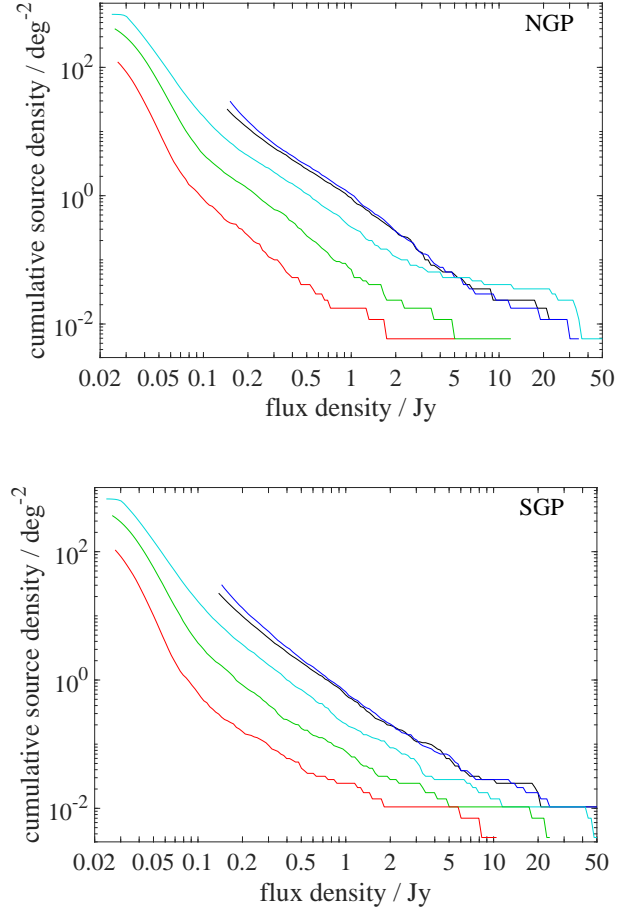
Figure 7. The cumulative number of sources as a function of flux density at $100\,\mu$m (black), $160\,\mu$m (blue), $250\,\mu$m(cyan), $350\,\mu$m (green) and $500\,\mu$m (red). The NGP area is shown in the top panel, and the SGP in the bottom panel. The counts are plotted only above the limit of 3σ in each wave band.

MADX to detect the sources and measure their flux densities and positions. The results of these "in-out" simulations apply to the NGP and SGP catalogues, which were produced using almost exactly the same methods.

We investigated the accuracy of the source positions in two ways: (1) by looking at the positional offsets between the *Herschel* sources and galaxies found on optical images; (2) from the in-out simulations. Bourne et al. (2016) and F17 describe the details of the first method, which takes account of the clustering of the galaxies in the optical catalogue and the PSF of the *Herschel* observations. Note that astrometric offsets were first calculated using catalogues from individual *Herschel* observations. The astrometry for each observation was updated before creating the final maps (S17).

In the case of the NGP, we applied this method using the galaxies found in the SDSS r-band images (F17), which thus ultimately ties the *Herschel* positions to the SDSS astrometric frame. In the case of the SGP, we used the galaxies found in the VLT Survey Telescope ATLAS (Shanks et al. 2015), which thus ultimately ties the astronometry in the SGP to the astrometric frame of this survey. We find that the positional error, $\sigma_{\rm pos}$, varies from 1.2 to 2.4 arc seconds as the signal-to-noise in flux varies from 10 to 5, with a relationship between positional accuracy and flux density given by $\sigma_{\rm pos} = 2.4({\rm SNR}/5)^{-0.84}$. This agrees well with the errors in the measured positions of the artificial sources in the in-out simulations (V16).

The mean positional errors as a function of position within the NGP and SGP fields are shown in Fig. 8. Though there are hints of systematic variations in different parts of the fields, these are around 1 arcsec, less than the quoted absolute pointing accuracy of *Herschel* of $\simeq 2$ arcsec (Pilbratt et al. 2010).

4.3. *Purity, flux boosting and completeness*

The catalogue is a 4-σ catalogue and so we can use Gaussian statistics to predict the number of sources that will actually be noise fluctuations; on this basis we expect $\simeq 0.2\%$ of the sources in the catalogue to be spurious. However, V16 argue that this is likely to be a significant overestimate because our errors, while being good estimates of the errors on the flux measurements, are likely to underestimate the signal-to-noise of a detection.

A major problem in submillimetre surveys, where source confusion is usually an issue, is flux bias or 'flux boosting', in which the measured flux densities are systematically too high. V16 used the in-out simulations to quantify this effect in the H-ATLAS. Table 6 in V16 gives estimates of the flux bias as a function of flux density for all three SPIRE bands. The table shows that at the 4σ detection flux density, the measured flux densities are on average higher than the true flux densities by $\simeq 20\%$, 5% and 4% at 250 μm, 350 μm and 500 μm, respectively. Astronomers interested in comparing the flux densities in the catalogue with the predictions of models should be aware of this effect. Table 6 in V16 can be used to correct the flux densities for this effect.

Note that the flux limit for significant PACS detections is much brighter than the confusion limit, and so PACS fluxes are not affected by confusion noise. Also the 250-μm noise is so much lower than the PACS noise, that the 250-μm selection should not introduce any sig-

nificant incompleteness in the PACS sample. The PACS sample should have completeness and purity as expected for the quoted Gaussian noise in the flux measurements.

V16 also used the in-out simulations to estimate the completeness of the survey as a function of measured flux density in all three SPIRE bands. This is shown in Figure 21 of V16 and listed in Table 7 of V16. The completeness at 250 μm is 87% at the 4σ detection limit of the survey.

5. SUMMARY

We have described the construction of the source catalogues from the *Herschel* survey of fields around the north and south Galactic poles. This survey which was carried out in five photometric bands – 100, 160, 250, 350 and 500 μm – was part of the *Herschel* Astrophysical Terahertz Large Area Survey (H-ATLAS), a survey of 660 deg^2 of the extragalactic sky. Our source catalogues cover 285 deg^2 around the SGP and 170 deg^2 around the NGP.

The catalogues contain 118,986 sources for the NGP field and 193.537 sources for the SGP field detected at more than 4σ significance in any of the 250 μm, 350 μm or 500 μm bands. We present photometry in all five bands for each source, including aperture photometry for sources known to be extended. We discuss all the practical issues - completeness, reliability, flux boosting, accuracy of positions, accuracy of flux measurements - necessary to use the catalogues for astronomical projects.
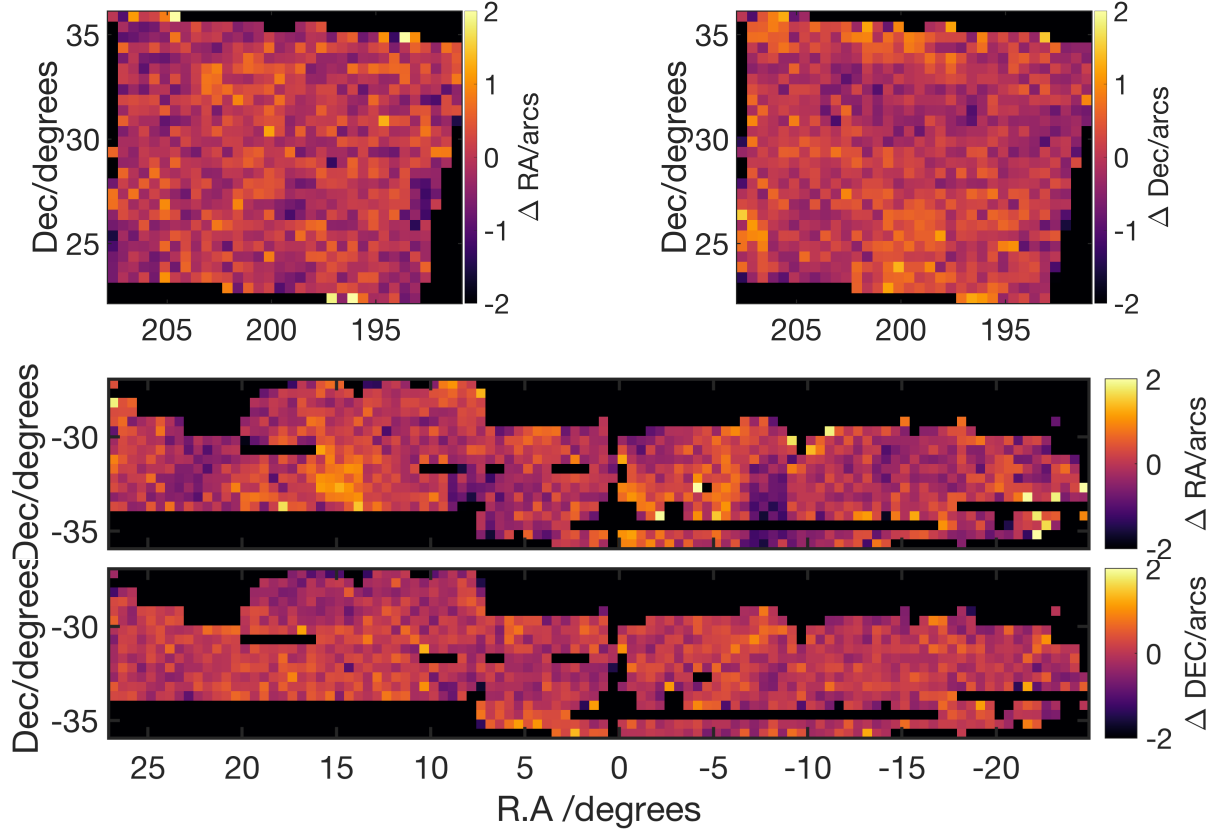
REFERENCES

Figure 8. The mean positional errors in R.A and Dec. averaged in areas 0.5 deg×0.5deg as a function of position on the sky for the NGP and SGP fields.

Bourne, N. et al. 2016, MNRAS, 462, 1714

Chapin, E.L. et al. 2011, MNRAS, 411, 505

Dunne, L. et al. 2011, MNRAS, 417, 1510

Eales, S., et al. 2010, PASP, 122, 499

Eales, S., et al. 2018, MNRAS, 473, 3507

Franceschini, A. et al 1991, A&AS, 89, 285

Fudamoto, Y. et al. 2017, MNRAS, 472, 2028

Furlanetto, C. et al. 2017, MNRAS, submitted (F17; Paper III)

Griffin, M.J. et al. 2010 A&A, 518, L3

Griffin, M.J. et al. 2013, MNRAS, 434, 992

Ibar, E., 2010, MNRAS, 409, 38

Neugebauer, G. et al. 1984, ApJ, 278, L1

Pascale, E., et al. 2011, MNRAS, 415, 911

Pearson, E.A. et al. 2013, MNRAS, 435, 2753

Pilbratt, G. L., et al. A&A, 518, L1

Planck Collaboration XXVI, 2016, A&A, 594, 26

Poglitsch, A., et al. 2010 A&A, 518, L2

Rigby, E.E, et al. 2011, MNRAS, 415, 2336

Shanks, T. et al. 2015, MNRAS, 451, 4238

Skrutskie et al. 2006, AJ 131, 1163

Smith, D.J.B. et al. 2011, MNRAS, 416, 857

Smith, M.W.L. et al. 2017, ApJ suppl., in press (S17; Paper I)

Valiante, E. et al. 2016, MNRAS, 462, 3146 (V16)

Valtchanov, I. (Ed.) 2017, The SPIRE Handbook, HERSCHEL-HSC-DOC-0798, v3.1

Zavala, J.A. et al. 2017, Nature Astronomy, in press (arXiv: 1707.09022)